# Determination of the structure of the recombinant *T* = 1 capsid of Sesbania mosaic virus

**V. Sangita*, S. Parthasarathy*, S. Toma†, G. L. Lokesh‡, T. D. S. Gowri‡, P. S. Satheshkumar‡, H. S. Savithri‡ and M. R. N. Murthy*,****

*Molecular Biophysics Unit and ‡Department of Biochemistry, Indian Institute of Science, Bangalore 560 012, India
†Institute of Protein Research, Osaka University, Osaka, Japan

**The recombinant coat protein (CP) of Sesbania mosaic virus lacking segments of different lengths from the N-terminus expressed in *E. coli* was shown to self-assemble into a variety of distinct capsids encapsidating 23S rRNA from the host and CP mRNA *in vivo*. Particles with 60 copies (*T* = 1) of protein subunits were observed when protein lacking 65 amino acids from the N-terminus was expressed. This recombinant protein possesses the sequence corresponding to the S-domain of the native, *T* = 3 icosahedral particles but lacks the *b*-annulus, the *b*A strand (residues 67–70) and the arginine-rich ARM motif (residues 28–36). Purified *T* = 1 particles crystallized in the monoclinic space group $P2_1$ with cell parameters of *a* = 188.4 Å, *b* = 194.6 Å, *c* = 272.1 Å and *b* = 92.6°. The structure of the *T* = 1 particles was determined by X-ray diffraction at 3.0 Å resolution. As expected, the polypeptide fold of the subunit closely resembles that of the S-domain of the native virus. The recombinant particles bind calcium ions in a manner indistinguishable from that of the native capsids. The structure reveals the major differences in the quaternary organization responsible for the formation of *T* = 1 against *T* = 3 particles.**

ICOSAHEDRAL arrangement of protein subunits is a common architecture of most spherical virus capsids[1]. X-ray crystal structures of several isometric viruses have provided insights into the nature of inter-subunit and protein–nucleic acid interactions. However, the mechanism of assembly of these particles is less clear. There is substantial variation in the nature of the interactions that govern the capsid stability among different spherical viruses, although the polypeptide folds might be similar[2]. For example, in tymoviruses, the capsid structure is stabilized by strong protein–protein interactions, reflected in the occurrence of empty protein shells *in vivo*[3–7]. On the other hand, empty capsids devoid of nucleic acid are rarely observed in members belonging to the sobemo-, bromo- and cucumovirus groups, where capsid stability appears to be dominated by protein–nucleic acid, metal-ion mediated and electrostatic interactions[8–12]. Since the nature of stabilizing interactions of icosahedral capsids varies significantly among different groups of viruses, it is likely that the mechanisms of assembly are also different.

SeMV is a small isometric plant virus that infects *Sesbania grandiflora*. It is comprised of a monopartite, single-stranded, positive-sense RNA genome of size 4149 nucleotides[13], encapsidated in an icosahedral protein shell made up of 180 identical coat protein (CP) subunits of 268 amino acids. The primary structure of the SeMV CP[14] has 62% identity with Southern cowpea mosaic virus (SCPMV, genus sobemovirus, earlier known as southern bean mosaic virus, cowpea strain), which is the type member of the sobemovirus group. The crystal structure of the SeMV determined at 3 Å resolution[15,16] revealed close similarity to that of SCPMV[17]. The chemically identical CP subunits in these viruses are present in three quasi-equivalent conformations designated as A, B and C (Figure 1). The A subunits interact at the icosahedral five-fold axes and form 12 pentamers. B and C subunits interact at the icosahedral three-fold axes to form 20 hexamers. No significant electron density was observed for the first 70 amino acids of the N-terminal region in A and B subunits in SeMV. However, the N-terminal arm of C-subunit was more ordered and the polypeptide could be traced from residue 44. The N-terminal arms of C-subunits interact with each other to form a structure called *b*-annulus (residues 48–51) that is believed to stabilize the capsid structure at the quasi-six-fold axes[18]. Structure determination of SeMV suggested the presence of four ion-binding sites in the asymmetric unit, three of which were found in the inter-subunit interfaces, AB, BC and CA and the fourth at the quasi three-fold axis[15,19]. The CPs of many icosahedral plant viruses with RNA genomes such as tomato bushy stunt virus[20]

**For correspondence. (e-mail: mrn@mbu.iisc.ernet.in)

(TBSV, genus tombusvirus), SCPMV[17], cowpea chlorotic mottle virus[21] (CCMV, genus bromovirus) and SeMV[15] have a highly basic N-terminal segment which is proposed to interact with the RNA stabilizing the capsid structure, neutralizing the negative charges on the RNA phosphates and probably providing a switch for $T = 3$ capsid formation. The N-terminus of SeMV consists of a motif RRRNRRRQR (residues 28–36), with seven arginine residues in a stretch of nine amino acids. This motif has been termed as the arginine-rich motif (N-ARM) and is also present in the CPs of other sobemoviruses, brome mosaic virus (BMV, genus bromovirus), cucumber mosaic virus (CMV, genus cucumovirus) and several other viral CPs[11]. It has recently been demonstrated that the deletion mutants that lack 22, 36 and 65 amino acid residues from the N-terminus of the SeMV CP expressed in *E. coli* assemble into recombinant capsids of varying sizes and structures[19]. These capsids were found to encapsidate 23S ribosomal RNA of host origin as well as RNA corresponding to CP messenger. Structural studies on the variety of assembly products of SeMV observed by Lokesh *et al.*[19] would provide valuable molecular information controlling the assembly of these particles. In the N65 deletion mutant, the residues involved in the formation of N-ARM as well as the *b*-annulus are absent and only $T = 1$ particles are formed. In this article we present crystal structure determination of $T = 1$ recombinant capsids obtained for the N65 deletion mutant (T1-SeMV) and contrast the salient features of its architecture to those of the $T = 3$ native SeMV capsids (T3-SeMV).

## Materials and methods

### *Crystallization of T = 1 particles of SeMV*

Production and purification of recombinant N65 deletion mutant were done using previously established procedures[19]. Native SeMV crystals were obtained using ammonium sulphate as the precipitant. However, the recombinant N65 deletion mutant did not give diffraction quality crystals under similar conditions. Therefore, new crystallization conditions were screened using the Hampton crystal screen 1. Several conditions containing PEG as the precipitant in the pH range 4.5 to 7.5 produced crystals of similar morphology. These conditions were further refined in the subsequent crystallization trials to the following three conditions: (a) 1 M sodium acetate (pH 5.5) in the presence of 0.18 M $Li_2SO_4$ with 4 to 8% PEG3350; (b) 1 M sodium acetate (pH 5.5) in the presence of 0.2 M $MgCl_2$ with 4 to 8% PEG3350, and (c) 1 M HEPES (pH 7.5) in the presence of 0.2M $MgCl_2$ with 4 to 8% PEG3350. Replacing PEG3350 by higher concentrations of PEG400 also produced good quality crystals. Crystals could be obtained using both hanging and sitting drop techniques. Capsid concentration was approximately

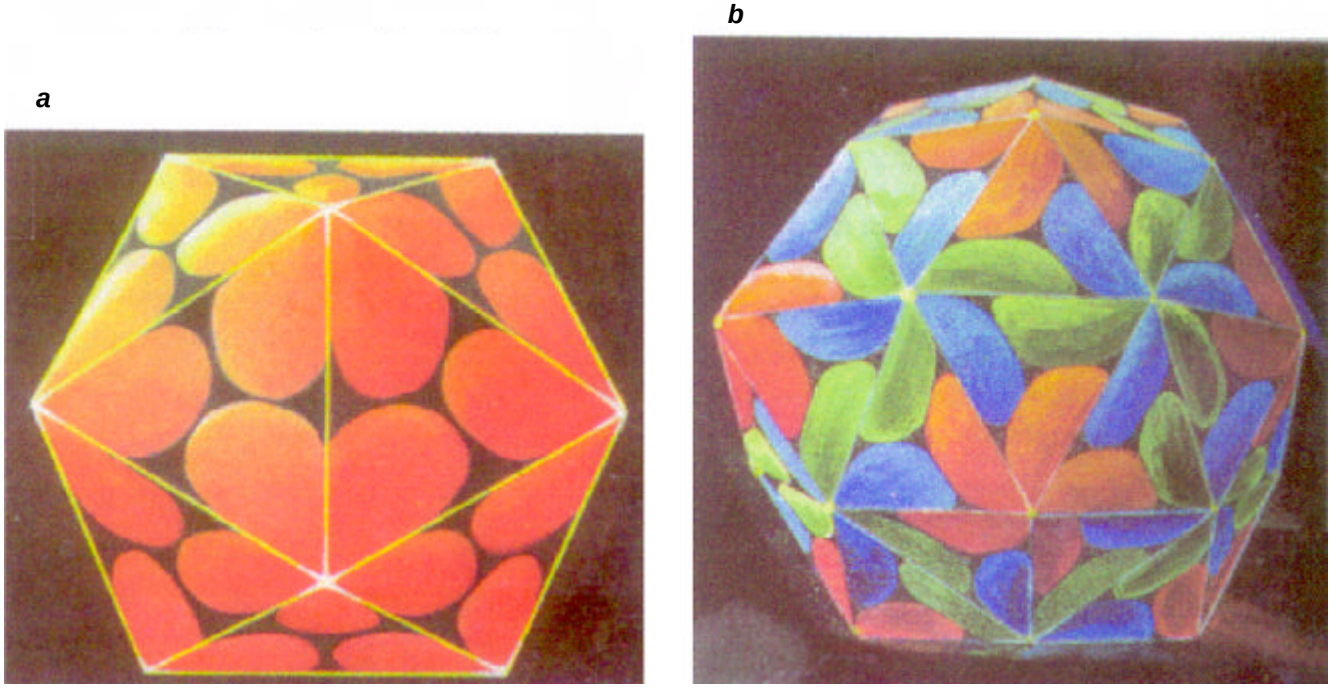


**Figure 1.** Arrangement of subunits in (***a***) $T = 1$ and (***b***) $T = 3$ icosahedral capsids of isometric viruses. All subunits of $T = 1$ capsids are in chemically identical environments. Subunits on $T = 3$ capsids, although identical in sequence, occur in three distinct environments. These subunits are designated A (red), B (blue) and C (green) following Harrison *et al.*[20]. The A (red) subunits form pentamers at the icosahedral five-fold axes, while B and C subunits form hexamers at the icosahedral three-fold axes.

8 mg/ml (assuming 5 O.D. = 1 mg/ml) and equal volumes of virus and reservoir solutions were mixed. While $MgCl_2$ conditions produced crystals within two days, crystals appeared in the presence of $Li_2SO_4$ after seven days with better morphology.

### *Data collection and processing*

The crystals were stable for months and unlike native virus crystals, did not lose crystallinity upon freezing to liquid nitrogen temperatures**.** Crystals were cryo-protected by equilibrating in 20% glycerol in the crystallization buffer for 5 to 10 min. Therefore, it was possible to collect diffraction data from a single crystal using an Oxford cryocooler operated at 100 K and a MAR 300 imaging plate detector mounted on a Rigaku RU-200 rotating anode X-ray generator equipped with a 200 μ focal cup. X-ray beam was focused using an Osmic mirror system. A total of 150 frames, each of 0.4° oscillation, were collected. The crystal to detector distance (*D*) was kept at 180 mm and each frame was exposed for 500 s with two passes. The data frames were indexed and the intensities were scaled using the DENZO/SCALEPACK suite of programs[22]. The continuous data frames were integrated in three sectors and scaled. The cell parameters and subsequent scaling indicated that the space group is monoclinic. Since sufficient number of axial *oko* reflections were not recorded, the space group ambiguity $P2/P2_1$ could not be resolved by systematic absences. The cell parameters are: **a** = 188.4 Å, **b** = 194.6 Å, **c** = 272.1 Å, *b* = 92.6°. The diameter of the particles as estimated by electron microscopy was about 190 Å. Two such particles are compatible with the monoclinic cell. Assuming the particles to have a diameter equal to the nearest inter-particle distance, the volume of the cell occupied by the spherical particles is 69.3%. Relevant data collection statistics are listed in Table 1.

### *Structure determination and refinement*

The icosahedral symmetry of the capsids was established by computation of rotation functions[23]. Self-rotation functions for *k* values of 72°, 120° and 180° were calculated using GLRF program[24]. These functions unambiguously established the particle orientation. Subsequent calculation of Patterson map provided information on the space group as well as particle position. A plausible model for the structure of the $T = 1$ particles was constructed starting from the structure of the native virus. The modelled structure was placed in the monoclinic cell using the results of rotation function and Patterson maps. The initial orientation and position of the particle were further improved by rigid-body refinement using X-PLOR[25]. This was done by manually changing the $k, f, j$, representing the orientation of the particle and translation vector, representing the position of the particle in small steps. Strict 60-fold non-crystallographic symmetry constraint corresponding to the icosahedral symmetry was applied throughout the refinement. Initial refinements were performed using reflection data between 20 and 5.0 Å resolution. For further refinement, reflection data were added in steps of 0.5 Å resolution. After getting the best possible orientation and position of the particle using X-PLOR, the model was subjected to further refinement using 'mlf' (maximum likelihood in amplitudes) option in CNS version 1.0 (ref. 26). In CNS refinements, complete data between 20.0 and 3.0 Å resolution were used after setting aside 5% of the data for cross-validation[27,28]. Anisotropic *B*-scaling and bulk solvent corrections were employed throughout the refinement. After initial rigid body and positional refinement, sigma-weighted $2F_o–F_c$ and $F_o–F_c$ maps[29] were calculated and visualized using the interactive model-building program O (ref. 30). Difference maps computed at this stage showed the electron density corresponding to the bound calcium ion also. A few more cycles of refinement, including the bound calcium ion were performed. Only the group *B*-factors corresponding to the main chain, side chain atoms and calcium ion were refined. Table 2 lists the relevant refinement statistics. Structures were analysed using the program PROCHECK[31] and superpositions with different capsomers of SeMV $T = 3$ structure were performed using the programs HOMO[32] and ALIGN[33]. Due to the 60-fold non-crystallographic symmetry in the asymmetric unit of the crystal, substantial further improvement of the elec-

**Table 1.** Data reduction statistics

| | |
|---|---|
| Radiation | $CuK_a$ |
| Space group | $P2_1$ |
| Resolution range (Å) | 20.0–3.0 |
| Total number of observations | 3,54,296 |
| Number of unique reflections | 2,08,778 |
| Overall completion | 53.5% |
| Multiplicity | 1.7 |
| *I*/Sig *I* | 7.7 |
| Overall $R_{sym}$[a] | 14.3 |

[a] $R_{sym} = 100 \times \Sigma |\langle I \rangle - I| / \Sigma \langle I \rangle$.

**Table 2.** Refinement statistics

| | |
|---|---|
| Refinement program | CNS_1.0 (Maximum likelihood in amplitudes) |
| Number of protein atoms | 1448 |
| Residues (of wild type protein) | 73–268 |
| Resolution range (Å**)** | 20.0–3.0 |
| Size of test set (%) | 5% |
| No. of reflections in working set | 1,77,424 |
| No. of reflections in test set | 1,95,65 |
| Initial *R* for the model | 50.2% |
| *R* and $R_{free}$ (final)% | 27.2 and 27.5 |
| Luzzati error (*R* and $R_{free}$) | 0.45 and 0.46 |
| RMSDs | |
| Bond length | 0.008 Å |
| Bond angle | 1.44° |

tron density is possible by density averaging and modification procedures. These computations are in progress.

## Results and discussion

### *Rotation function studies*

Earlier studies[13] had established that the N65 mutant CP of SeMV assembles into $T = 1$ particles with a sedimentation coefficient of 52S and a particle diameter of approximately 19 nm. These $T = 1$ particles were crystallized and X-ray diffraction data collected on the crystals as described in the materials and methods. In order to establish the particle symmetry, rotation functions[23] were calculated.

Figure 2 shows the $k = 72°$ hemisphere of rotation function. Since there are two particles in the unit cell, two sets of six peaks each corresponding to the two particles were anticipated. However, only one set of icosahedral symmetry axes was observed. This suggests that the two icosahedral particles have nearly identical orientations. Accordingly, one of the particle two-folds was found to be parallel to the crystallographic 2 or $2_1$ axis. Rotation function for $k = 180°$ and $k = 120°$ hemispheres (not shown) were consistent and revealed only one set of peaks.

Examination of the $K = 72°$ hemisphere indicates that one of the five-fold axes is aligned along the crystallographic *a* axis (Figure 2). Thus, the particle orientation is such that one of its icosahedral two-folds is along crystal *b* and a five-fold is along *a*. These two assignments completely determine the orientation of the particle in the unit cell. The refinement program X-PLOR uses an orthogonal system in which the monoclinic *b* is parallel to orthogonal *Y*, monoclinic *a* is parallel to orthogonal *X* and monoclinic *c** is parallel to orthogonal *Z*. Therefore, the mutually perpendicular *a*, *b*, *c** axes (X-PLOR orthogonal system) are related to the Cartesian system based on the 222 symmetry of the icosahedral particle (PQR system)[20] by a rotation about the crystal *b* axis by an angle equal to the angle between the nearest two-fold and five-fold axes of the icosahedron. This angle is 31.72°. The matrix that defines this rotation is therefore,

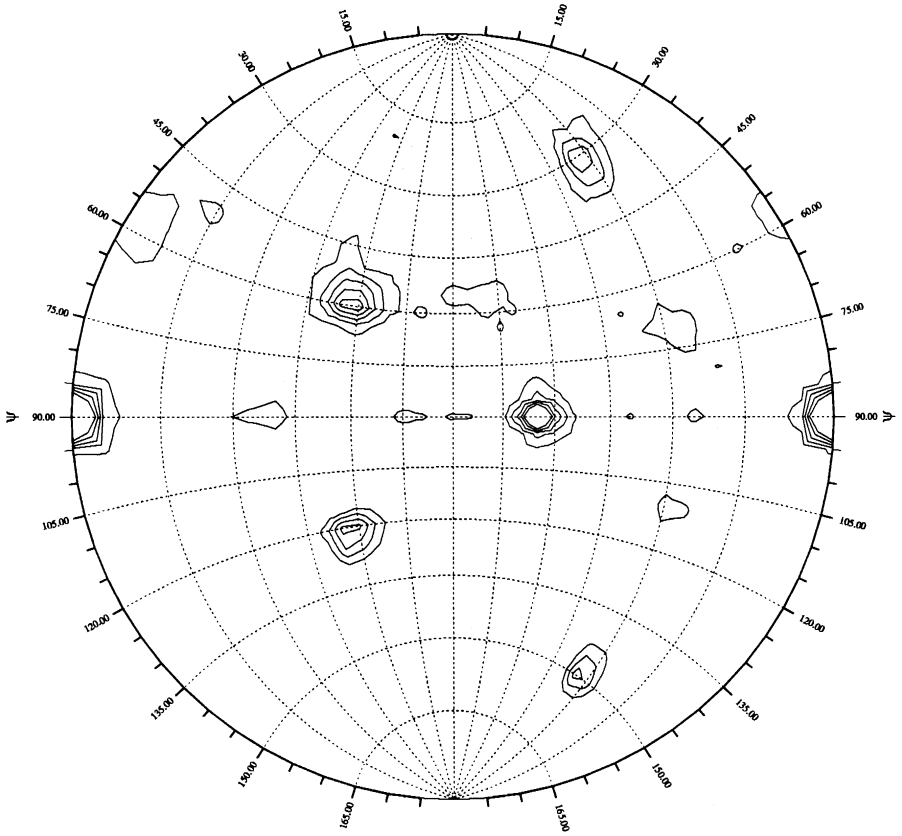


**Figure 2.** $k = 72°$ hemisphere of rotation function of T1-SeMV calculated using reflections in 5.5–10 Å resolution shell. The radius of integration was 90 Å. About 774 terms larger than three times the mean intensity were used to represent the second Patterson function. Only one set of peaks related by icosahedral symmetry might be observed, suggesting that the two particles of the monoclinic cell are similarly oriented. The contours are drawn at intervals of 1 *s* starting from 1 *s* above the mean background.

| 0.85065 | 0.00000 | – 0.52573 |
|---|---|---|
| 0.00000 | 1.00000 | 0.00000 |
| 0.52573 | 0.00000 | 0.85065 |

### *Determination of particle position*

Since the two particles in the unit cell are likely to have similar orientations, vectors joining corresponding atoms of the two particles will all be nearly parallel and equal to the inter-particle vector leading to a large peak in the Patterson function. If the space group is P2, the vectors will result in a large peak in the $v = 0$ Patterson section, while space group $P2_1$ will result in a large peak in the $v = 1/2$ Patterson section. In either case, the Patterson peak will be at $u = 2x$, $w = 2z$, where $x$ and $z$ are the positional coordinates of a particle centre. Therefore, a native Patterson map was calculated in different resolution shells. A very large peak was observed only in the section $v = 1/2$, suggesting the space group to be $P2_1$. The peak was at 484 standard deviations in units of RMS above the mean background of Patterson values for the resolution range 15.0–5.0 Å and 241 standard units above the mean in the resolution range 3.5–5.5 Å. The particle position suggested by both these peaks is $x = 0.2406$, $z = 0.2542$.

Since the particle two-fold is almost exactly parallel to the crystallographic two-fold and the particle positions are close to (¼, 0, ¼) and (¾, ½, ¾), the crystal intensity statistics could show the character of a body-centred cell. Therefore, the mean intensities of all parity groups were examined. However, no significant difference in the mean intensities was observed between $h + k + l$ = even and odd reflections, indicating that the particle position is either not exactly (¼, 0, ¼) or its two-fold is not exactly orientated parallel to the crystal two-fold axis (crystal *b*). The particle position and orientation were, therefore, further refined using X-PLOR as described later.

### *Generation of approximate coordinates of a subunit in the X-PLOR orthogonal system*

The structure of the native SeMV known at 3 Å resolution[15,16] was used as the starting point for the construction of a plausible model for T1-SeMV. It was straightforward to generate a densely packed $T = 1$ capsid (as evaluated by usual inspection) starting from 12 pentamers of the T3-SeMV (particle diameter 30 nm) by rotations of pentamers followed by translations towards the particle centre. The rotation required about the five-fold was 36° (half the throw angle of the five-fold symmetry). Translation of pentamers by 64 Å towards the viral centre resulted in close packing of the pentameric units without steric repulsion and the diameter of the resulting capsid was in close agreement with the observed value (19 nm). This model closely resembles the experimentally determined structure of SBMV $T = 1$ particle[34]. These transformations retain the inter-subunit contacts of the pentamer found in T3-SeMV. In contrast, well-packed $T = 1$ structures could not be generated using 30 icosahedral dimeric units of the $T = 3$ capsid. It was found that the crystallographic dimer and trimer of the $T = 1$ capsid closely resemble the quasi dimer and trimer of the $T = 3$ particles. The coordinates of the subunits so generated refer to the PQR system based on three mutually perpendicular two-fold axes of the icosahedron defined by Harrison *et al.*[20]. The resulting coordinates of the subunit were then transformed to the X-PLOR orthogonal system by the transformation specified by the matrix obtained by rotation function results followed by the translation of (42.26 Å, 0.0 Å, 69.08 Å) obtained from Patterson function calculations. This places the coordinates of the $T = 1$ particle at approximately the correct position and orientation with respect to the orthogonal system used by X-PLOR. Further, refinement of the position as well as the orientation of the icosahedral $T = 1$ particle could be achieved by X-PLOR.

### *Refinement using X-PLOR*

As there is a full virus particle in the crystallographic asymmetric unit, there are 60 non-crystallographic symmetry operators, which could be exploited in the refinement with X-PLOR. The icosahedral symmetry operators are given by rotations $PR\,P^{-1}$ and translations $(T\text{-}PR\,P^{-1}(T))$, where $R$ refers to the 60 non-crystallographic (icosahedral) symmetry transformations in PQR system, P refers to the transition matrix between PQR and X-PLOR systems and corresponds to a rotation of $(j, f, k) = (0.0°, 0.0°, 31.72°)$; translation $T$ is approximately given by fractional to orthogonal transformation of (0.24062, 0.0, 0.25417) = (42.26 Å, 0.0 Å, 69.08 Å).

A program was written to generate the 60 matrices varying $(j, f, k)$ around values (0.0, 0.0, 31.72), respectively and $T$ around (42.26, 0.0, 69.08), as suggested by the rotation and Patterson functions. Rigid-body refinement was carried out using X-PLOR. The lowest R-factor of 38.9 was obtained for $(j, f, k) = (1.75°, 45.0°, 32.93°)$ and $T_x, T_z$ = (42.1366 Å, 69.2458 Å). Further refinement of particle positions reduced the $R$-factor to 27.2% and $R_{free}$ to 27.5%. The quality of the final electron density map is illustrated in Figure 3. Electron density was poorly defined for 16 residues. These include several residues of the internal loop (160–178), which had high B-values in the native $T = 3$ structure. The final model has reasonable stereochemistry as seen by the Ramachandran plot[35] (not shown here). The final refinement statistics are shown in Table 2.

A difference Fourier calculated at this stage (Figure 4) revealed a single ion in the icosahedral asymmetric unit.

The density shown in Figure 4 was assumed to represent a bound calcium ion by comparison with the native structure.

### *Subunit structure and organization*

The polypeptide fold of the subunit in the icosahedral asymmetric unit is shown in Figure 5. As anticipated, the polypeptide fold closely resembles that of T3-SeMV. The subunit structure consists of an eight-stranded anti-parallel *b*-barrel (*b*B-*b*H, residues 73–268 corresponding to the S-domain of T3-SeMV). A few residues that were built as alanines due to poorly defined electron density in T3-SeMV could be modelled in the T1-SeMV map. In the T1 particle, all subunits participate in pentameric, trimeric and dimeric interactions at the icosahedral five-fold, three-fold and two-fold axes, respectively (Figure 1). Five subunits interacting at the icosahedral five-fold axis are structurally equivalent to the pentameric A subunits of $T = 3$ native virus. The A, B and C subunits of the icosahedral asymmetric unit related by an approximate or quasi three-fold symmetry of the $T = 3$ virus are similar to the trimeric cluster of the $T = 1$ particle related by the icosahedral three-fold axis. There are two distinct types of dimers in the $T = 3$ capsid (Figure 1). The CC2 dimers are related by an exact icosahedral two-fold axis, while the AB5 dimers are related by a quasi two-fold axis. There is only one type of dimeric unit in T1-SeMV, the subunits related by the icosahedral two-fold.

Figure 6 illustrates the residual differences in the positions of C*a* atoms of a number of subunits related by

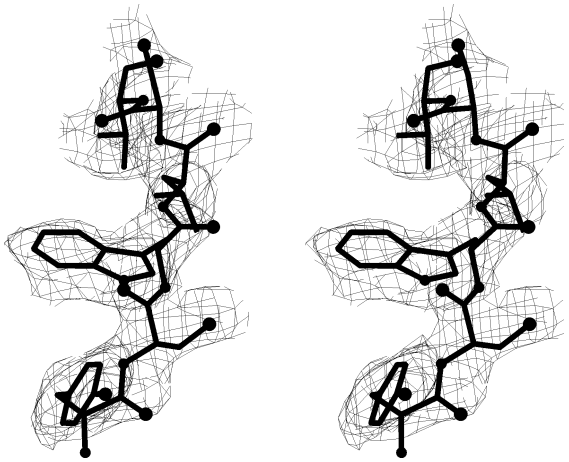

**Figure 3.** Section representing the quality of the final electron density map of T1-SeMV. Contours are at 1.0 *s*.

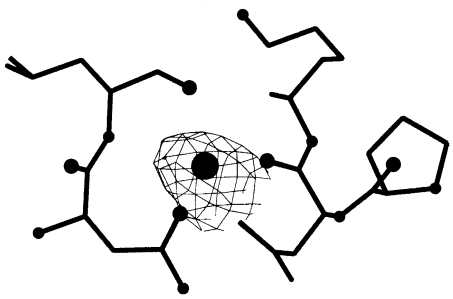

**Figure 4.** Difference Fourier section, contoured at 2.5 *s*, showing the electron density for a bound ion. The ion was identified as a calcium ion by comparison with the T3-SeMV structure.

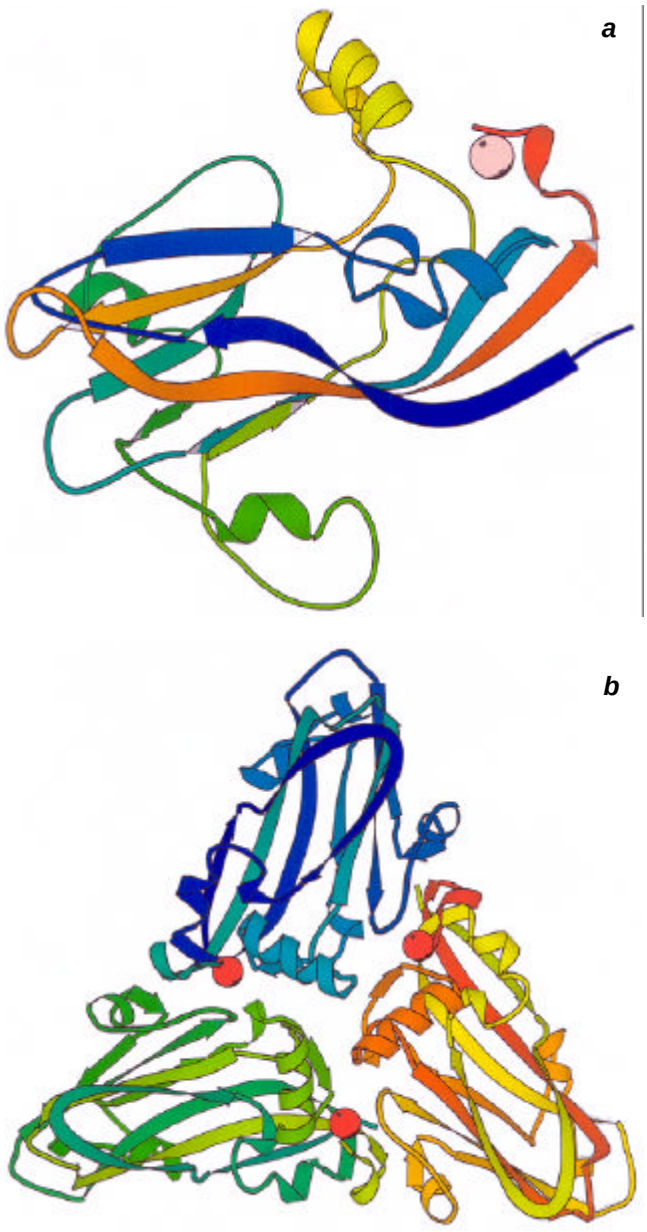


**Figure 5.** ***a***, Ribbon diagram illustrating the polypeptide fold of T1-SeMV (residues 73–268 of the native particles) protein. The polypeptide is coloured with blue at the amino terminus and changes gradually to red at the carboxy terminus. Calcium is shown as a sphere; ***b***, Spatial arrangement of three protein subunits in an icosahedral facet of T1-SeMV. The three subunits are coloured differently for clarity, although, unlike in $T = 3$ native particles, they are chemically and structurally identical.

icosahedral symmetry axes after the superposition of a pentameric subunit of $T = 1$ and $T = 3$ structures. It is clearly seen that the quaternary organization of the subunits across the icosahedral two-fold axes is very different, while the quasi two-fold relation in $T = 3$ and icosahedral two-fold in $T = 1$ as well as the relation between neighbouring subunits of the pentamers are closely similar. The overall RMS difference is for the C$\alpha$ atoms of the superposed subunits 0.37 Å. Largest difference is observed for the internal helix $a$-C and the associated loop. This helix facing the RNA interior is somewhat disordered in the structure of the native virus. This probably reflects the different RNA interactions in the two capsids. Similarly, a few residues only partially ordered or disordered in the native virus appear to be ordered in the $T = 1$ particles. However, no significant density corresponding to RNA is discernible.

### *Putative calcium-binding sites*

A putative ion located in the icosahedral asymmetric unit of T1-SeMV is bound at the inter-subunit interface of subunits related by the icosahedral three-fold axis. The ion is at a distance of 77.46 Å from the particle centre. Three of these ions related by icosahedral symmetry are equivalent to the calcium ions related by the quasi three-fold axis in $T = 3$ particles, which are at distances of 136.7 Å, 131.9 Å, 135.6 Å, in the A, B and C subunits respectively from the virus centre[16]. As in the native particles, five ligands to the metal atom emanating from the protein subunits could be identified. The ligands are carboxylate oxygens from the side chains of Asp 146 and Asp149. A 12-residue segment around these residues is the most conserved region in sobemoviruses. Main chain carbonyl oxygens of Tyr 205, Asn 267 and amide oxygen of Asn 268 are the ligands contributed by the subunit related by icosahedral three-fold symmetry.

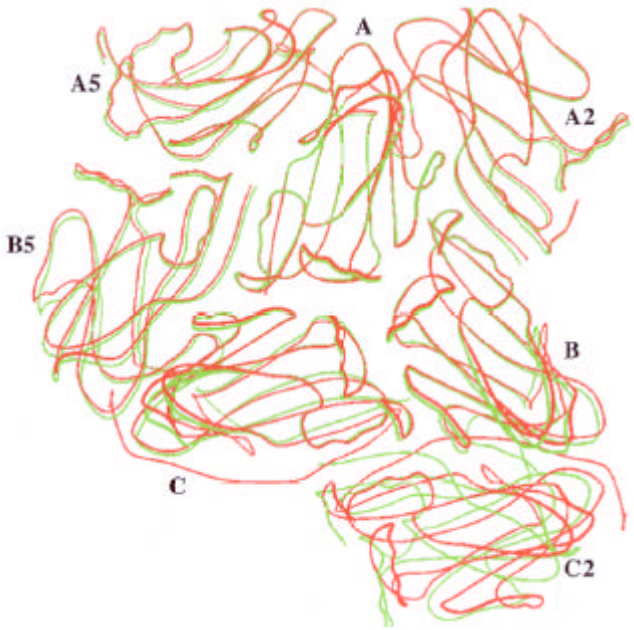


**Figure 6.** Illustration of the residual differences in the positions of C$\alpha$ atoms of subunits related by various icosahedral symmetry axes after the superposition of a pentameric subunit of $T = 1$ and $T = 3$ structures. The subunits of $T = 1$ recombinant capsid are shown in green while those of $T = 3$ native particles are in red.

### *Comparison of the subunit organization in T = 1 and T = 3 structures*

Comparisons were made with respect to changes in the quaternary organization of dimeric, trimeric and pentameric units of $T = 1$ SeMV capsids and $T = 3$ native particle structures. If S1(T1) and S2(T1) are two subunits in T1-SeMV and S1(T3) and S2(T3) are the corresponding subunits in T3-SeMV, the transformation required to superpose S1(T1) on S1(T3) was determined using HOMO. The resulting matrix was used to transform both S1(T1) and S2(T1) to S1′(T1) and S2′(T1). If the inter-subunit organization of S1 and S2 subunits in T1-SeMV and T3-SeMV is identical, S2′(T1) will also superpose S2(T3) by this transformation. Differences in the position and orientation of S2′(T1) and S2(T3) were therefore evaluated as the quantitative measure of the difference in the quaternary organization of S1 and S2 subunits in the two capsids.

It was found that the pentameric structure in the native virus and T1-SeMV is very similar. After superposition of one of the subunits of the pentameric capsomere, the residual transformation required to superpose the neighbouring subunits as described above corresponds to a rotation of 2.0° and a translation of 0.7 Å. Similarly the icosahedral trimer of the T1-SeMV and the quasi trimer of the native virus are very similar. The residual superposition in this case corresponds to rotations and translations of (4.1°, 1.1 Å) for the B subunit and (5.8°, 1.3 Å) for the C subunit. In contrast to a single dimeric species generated by an icosahedral two-fold in the $T = 1$ structure, the $T = 3$ capsids contain both icosahedral (CC2) and quasi two-fold (AB5; Figures 1 and 6) related subunits. Only the quasi two-fold-related dimeric structure of the native particle has a quaternary organization similar to the dimeric structure of the T1-SeMV. The organization of the icosahedral dimer of $T = 3$ is substantially different from the dimer of T1-SeMV. The residual transformations for selected pairs of subunits of $T = 3$ and $T = 1$ SeMV are shown in Table 3.

## Conclusions

The results of the present analysis are in agreement with the observations of Erickson *et al.*[34] on the structure of

**Table 3.** Comparison of the spatial relationship of selected subunit pairs in T1-SeMV and T3-SeMV. A pentameric subunit of T1-SeMV was superposed on the A subunit of T3-SeMV. The resulting transformation was used on all the subunits of T1-SeMV. For each pair of subunits in T1-SeMV, one of which was the subunit used for superposition, the residual transformation required for the superposition of the second subunits in the T1-SeMV and the corresponding subunit of T3-SeMV was evaluated. The values in columns 4 and 5 represent the residual rotation and translation between the second subunits

| Pair in $T = 3$ SeMV | Nature of pair in $T = 1$ SeMV | Nature of pair in $T = 3$ SeMV | Residual rotation (degrees) | Residual translation (Å) |
|---|---|---|---|---|
| AA5 | Pentamer | Pentamer | 2.0 | 0.7 |
| AB | Icosahedral trimer | Quasi trimer | 4.1 | 1.1 |
| AC | Icosahedral trimer | Quasi trimer | 5.8 | 1.3 |
| CC2 | Icosahedral dimer | Icosahedral dimer | 38.4 | 8.2 |
| AB5 | Icosahedral dimer | Quasi dimer | 5.0 | 1.3 |

$T = 1$ particles of SBMV, homologous to the present SeMV. However, the earlier result was limited to low resolution. Recently, the crystallization and preliminary X-ray diffraction data collection have been reported for the $T = 1$ capsids of BMV, although no detailed structure has been reported thus far[36]. Therefore, the present results provide detailed information on the oligomeric structures of dimeric, trimeric and pentameric units of the $T = 1$ and $T = 3$ particles constituted from the capsid protein of the same virus at a much higher resolution.

The limited resolution of SBMV T1 capsids reported earlier[34] is probably due to the fact that the truncated CP was obtained by trypsinization of the native protein, and hence it is likely that the resulting product was not entirely homogenous in size. In the present case, N65 SeMV was obtained by expressing the CP gene corresponding to the truncated protein in *E. coli* and hence is homogenous, reflecting the use of recombinant DNA technology in assembly studies on viral capsids.

Assembly studies on the deletion mutants of SeMV by Lokesh *et al.*[19] have clearly demonstrated that the N-terminal arm in SeMV CP plays a distinctive role in the assembly of the capsids compared with those of BMV, CMV, CCMV and PhMV. Removal of the N-ARM along with the *b*-annulus resulted in the formation of $T = 1$ particles. These $T = 1$ particles also encapsidated degraded 23S rRNA and a small amount of CP mRNA, suggesting the presence of sites outside the N-terminal 73 residues that are involved in RNA–protein interactions. Increased stain penetration of ethidium bromide and increased sensitivity to RNase with EDTA treatment in these particles suggest that their stability is mediated by metal ion-mediated interactions as in T3-SeMV[19]. The present results support these earlier observations and reveal that the metal ion is bound to the $T = 1$ particle in a manner indistinguishable from the mode of binding to the native particles, in spite of the large reduction in the overall diameter of the particles from 30nm in the $T = 3$ native particle to 19 nm.

What are the molecular interactions responsible for the formation of $T = 3$ as against $T = 1$ capsid structures? It has not been possible to arrive at an unequivocal answer from observations on the structures of $T = 3$ particles. Calcium ions found bound to the $T = 3$ capsids cannot be the reason, as they are also bound in an identical fashion to $T = 1$ particles. The icosahedral dimeric and pentameric subunit organization in T1-SeMV closely resembles the arrangements found in the quasi dimer and icosahedral pentamer of $T = 3$ SeMV. The major difference between the two particles lies with the icosahedral dimers. The residual transformation of these pairs was found to be 38.4° and 8.2 Å (Table 3). The ordered N-terminal arm of the C-subunits of T3 SeMV that are disordered in the A and B subunits is sandwiched between two C subunits and forms part of the sheet structure that extends from one subunit to another subunit across the icosahedral two-fold axis. Therefore, it has been suggested that the determinant of the $T = 3$ as against $T = 1$ structure is this arm[18]. The arm is missing in the $T = 1$ structure constructed from truncated protein. However, the ordered part of the N-terminus cannot by itself account fully for the formation of the $T = 3$ structure as elimination of the N-ARM motif, which is outside the ordered N-terminal segment also prevents formation of the $T = 3$ structure[13].


1. Caspar, D. L. D. and Klug, A., *Quant. Biol*., 1962, **27,** 1–24.
2. Rossmann, M. G. and Johnson, J. E., *Annu. Rev. Biochem*., 1989, **58,** 533–573.
3. Kaper, J. M., *Dissociation and Assembly*, North-Holland Publishing Co., Amsterdam, 1975.
4. Bouley, J. P., Briand, J. P. and Witz, J., *Virology*, 1977, **78,** 425–432.
5. Keeling, J., Collins, E. R. and Matthews, R. E. F., *ibid*, 1979, **97,** 100–111.
6. Keeling, J. and Matthews, R. E. F., *ibid*, 1982, **119,** 214–218.
7. Savithri, H. S., Munshi, S. K., Suryanarayana, S., Divakar, S. and Murthy, M. R. N., *J. Gen. Virol*., 1987, **68,** 1533–1542.
8. Savithri, H. S. and Erickson, J. W., *Virology*, 1983, **126,** 328–335.
9. Lane, L. C. in *Plant Virus Infections and Comparative Diagnosis* (ed. Kurstak, E.), Elsevier/North-Holland Biomedical Press, Amsterdam, 1981, pp. 333–376.
10. Rao, A. L. N. and Grantham, G. L., *Virology*, 1996, **226,** 294–305.
11. Schmitz, I. and Rao, A. L. N., *ibid*, 1998, **248,** 323–331.

12. Zlotnick, A., Aldrich, R., Johnson, J. M., Ceres, P. and Young, M. J., *ibid*, 2000, **277,** 450–456.
13. Lokesh, G. L., Gopinath, K., Satheshkumar, P. S. and Savithri, H. S., *Arch. Virol*., 2001, **146,** 209–223.
14. Gopinath, K., Sundareshan, S., Bhuvaneswari, M., Karande, A., Murthy, M. R. N., Nayudu, M. V. and Savithri, H. S., *Indian J. Biochem. Biophys*., 1994, **31,** 322–328.
15. Bhuvaneshwari, M., Subramanya, H. S., Gopinath, K., Savithri, H. S., Nayudu, M. V. and Murthy, M. R. N., *Structure*, 1995, **3,** 1021–1030.
16. Murthy, M. R. N., Bhuvaneswari, M., Subramanya, H. S., Gopinath, K. and Savithri, H. S., *Biophys. Chem.*, 1997, **68,** 33–42.
17. Abad-Zapatero, C. *et al.*, *Nature*, 1980, **286,** 33–39.
18. Sorger, P. K., Stockley, P. G. and Harrison, S. C., *J. Mol. Biol*., 1986, **191,** 639–658.
19. Lokesh, G. L., Gowri, T. D. S., Satheshkumar, P. S., Murthy, M. R. N. and Savithri, H. S., *Virology*, 2001, **292,** 211–223.
20. Harrison, S. C., Olson, A. J., Schutt, C. E., Winkler, F. K. and Bricogne, G., *Nature*, 1978, **276,** 368–373.
21. Speir, J. A., Munshi, S., Wang, S., Baker, T. J. and Johnson, J. E., *Structure*, 1995, **3,** 63–78.
22. Otwinowski, T. and Minor, W., *Methods Enzymol.*, 1997, **276**, 581–593.
23. Rossmann, M. G. and Blow, D. M., *Acta Crystallogr*., 1962, **A15,** 24–31.
24. Tong, L and Rossmann, M. G., *ibid*, 1996, **A46,** 783–792.
25. Brunger, A. T., X-PLOR, Version 3.1, A system for X-ray crystallography and NMR, Yale University, New Haven, CT, 1992a.
26. Brunger, A. T. *et al.*, *Acta Crystallogr*., 1998, **D54,** 905–921.
27. Brunger, A. T., *Nature*, 1992b, **355,** 472–475.
28. Kleywegt, G. J and Brunger, A. T., *Structure*, 1996, **4,** 897–904.
29. Read, R. J., *Acta Crystallogr*., 1986, **A42,** 140–149.
30. Jones, T. A., Zou, J-Y., Cowan, S. W and Keildgaard, M., *ibid*, 1991, **A47,** 753–770.
31. Laskowski, R. A., MacArthur, M. W., Moss, D. S. and Thornton, J. M., *J. Appl. Crystallogr*., 1993, **26**, 283–291.
32. Rossmann, M. G. and Argos, P., *J. Biol. Chem*., 1975, **250,** 7525–7532.
33. Cohen G. E., *J. Appl. Crystallogr*., 1997, **30,** 1160–1161.
34. Erickson, J. W., Silva, A. M., Murthy, M. R. N., Fita, I. and Rossmann, M. G., *Science*, 1985, **229,** 625–629.
35. Ramachandran, G. N and Sasisekharan, V, *Adv. Protein Chem*., 1968, **23,** 283–437.
36. Lucas, R. W., Kuznepsov, Y. G., Larson, S. B. and McPherson, A., *Virology*, 2001, **286,** 290–303.

ACKNOWLEDGEMENTS. This work was supported by a grant from the Department of Science and Technology, Govt of India. We thank staff in the X-ray laboratory and workshop, the Bioinformatics Centre and Supercomputing Education and Research Centre, IISc for help during the course of these investigations. V.S. and S.P. were supported by a CSIR fellowship.

Received 15 March 2002; revised accepted 13 April 2002

# Chemical composition of rainwater around an industrial region in Mumbai

**Medha S. Naik*, G. A. Momin, P. S. P. Rao, P. D. Safai and K. Ali**

Indian Institute of Tropical Meteorology, Pashan, Pune 411 008, India

**Chemical analysis of rainwater samples collected at Kalyan, a downwind location of a large industrial belt, and at Alibag and Colaba, the upwind locations, during the southwest monsoon seasons of 1994 and 1995 and comparison with similar data of 1973–74 reveal that pH of rainwater at Kalyan which was alkaline 20 years ago became acidic due to long-term effect of pollutants. A decreasing trend in excess $SO_4$ was observed at Colaba and Kalyan, which is attributed to the pollution control measures adopted by industries and switching over from coal to natural gas which contains low sulphur. Whereas the increasing trend in $NO_x$ observed at Kalyan and Colaba, is attributable to increased automobile emission.**

RAINWATER serves as a collector of many minor constituents of the atmosphere. Hence, the results of rainwater analysis help to reveal the chemical state of the air in which the rain-bearing clouds have formed. In addition, chemical composition of rain plays a critical role in defining the level of acid deposition and the state of some important bio-geochemical cycles of the earth–atmosphere system.

Sulphur dioxide and nitrogen dioxide emitted by burning of coal, natural gas, fuel oil and petrol, are oxidized and hydrolysed to sulphuric acid and nitric acid which subsequently give rise to acid rain. The acid content of rain in many parts of the world has steadily risen for the past several years, as the countries have become more and more industrialized and have increased the use of fossil fuel. Vast areas of the northern hemisphere, including Central Europe, Scandinavia, Northeast United States and Canada have been reported to be affected by acid rain. Asia is a region of rapid population growth and industrialization, and one with increased requirement for energy. Thus industrial development and higher standards of

*For correspondence. (e-mail: ms-naik@tropmet.res.in)